Stepping stone sampling for retrieving artifact-free electroencephalogram during functional magnetic resonance imaging

Kimitaka Anami,[a,*] Takeyuki Mori,[a,b] Fumiko Tanaka,[c] Yusuke Kawagoe,[d] Jun Okamoto,[e] Masaru Yarita,[f] Takashi Ohnishi,[c] Masato Yumoto,[a,g] Hiroshi Matsuda,[c] and Osamu Saitoh[a]

[a] *Department of Psychiatry, National Center Hospital for Mental, Nervous, and Muscular Disorders,*
National Center of Neurology and Psychiatry, Tokyo 187-8551, Japan
[b] *Department of Neuropsychiatry, Tokyo University Hospital, Tokyo, Japan*
[c] *Department of Radiology, National Center Hospital for Mental, Nervous, and Muscular Disorders,*
National Center of Neurology and Psychiatry, Tokyo 187-8551, Japan
[d] *Physio-Tech Co., Ltd., Tokyo 101-0032, Japan*
[e] *Siemens-Asahi Medical Technologies Ltd., Tokyo 141-8644, Japan*
[f] *Nihon Kohden Corp., Tokyo 161-8560, Japan*
[g] *Department of Clinical Laboratory, Tokyo University Hospital, Tokyo, Japan*

Received 21 June 2002; accepted 10 December 2002

Abstract

Ballistocardiogram and imaging artifacts cause major interference with simultaneous electroencephalogram (EEG) and functional magnetic resonance imaging (fMRI) recording. In particular, the large amplitude of the imaging artifact precludes easy retrieval of EEG signals during fMRI scanning. Recording with 20,000-Hz digitization rate combined with 3000-Hz low-pass filter revealed the real waveform of the imaging artifact, in which it was elucidated that each artifact peak precisely corresponded to each gradient component and actually had differential waveforms of the original gradient pulses. Based on this finding, to retrieve EEG signal during fMRI acquisition, a blip-type echo planar sequence was modified so that EEG sampling might be performed at every 1000 μs (digitization rate 1000 Hz) exclusively in the period in which the artifact resided around the baseline level. This method, called "stepping stone sampling," substantially attenuated the amplitude of the imaging artifact. The remnant of the artifact was subtracted from the averaged artifact waveform. In human studies, α activity was successfully retrieved by inspection, and its attenuation/augmentation was observed during eyes open/closed periods. Fast Fourier transform analysis further revealed that even from DC up to 120 Hz, retrieved EEG data during scanning had very similar power distributions to the data retrieved during no scanning, implying the availability of the high-frequency band of the retrieved EEG signals, including even the γ band.
© 2003 Elsevier Science (USA). All rights reserved.

Introduction

Positron emission CT and single photon emission CT have made it possible to map brain functional activities during various cognitive tasks in terms of brain metabolism and hemodynamics. These imaging techniques, however, cannot yet evaluate discrete neural correlates exclusively related to task execution because of their poor time resolution, and therefore their task-relatedness remains to be better defined. The advent of functional magnetic resonance imaging (fMRI) has improved the situation due to its fairly good temporal and anatomical resolution (Belliveau et al., 1991). On the other hand, currently available electrophysiological tools of electroencephalogram (EEG) and magnetoencephalogram facilitate evaluation of human cognitive activities with a time precision of milliseconds, far surpassing the above-mentioned imaging techniques. Therefore, parallel EEG recording with fMRI acquisition provides a

* Corresponding author. Dept. of Psychiatry, National Center Hospital for Mental, Nervous, and Muscular Disorders, National Center of Neurology and Psychiatry, 4-1-1, Ogawahigashi-cho, Kodaira, Tokyo 187-8551, Japan. Fax: +0081-42-346-1734.

E-mail address: anami@ncnpmusashi.gr.jp (K. Anami).

statistical model of the time course changes of each EEG event applicable to the fMRI volume train, with which the neural correlate of the EEG event can be mapped onto the high-resolution brain tomographic/surface view. This methodology should find wide application, ranging from neurophysiological to clinical investigations. However, simultaneous EEG/fMRI recording has been associated with some serious problems, among which the most critical are two artifacts manifest on the EEG. The first of these is the cardiac-related artifact whose amplitude is up to around 200 μV that emerges in synchronization with the cardiac pulse (Allen et al., 1998). Two possible causes of this artifact have been proposed: an electromotive force (Faraday's law) and a blood flow effect (Allen et al., 1998). Several methods have been devised to reduce this artifact such as use of a spatial filter (Bonmassar et al., 1999) and average subtraction (Allen et al., 1998). We substantially reduced the amplitude of this artifact to an acceptable level in many cases by employing a vacuum cushion system that could fix the subject's head and conform to the individual head shape (Anami et al., 2002). Based on the fact that appropriate suppression of head microvibration can largely remove the artifact, we thought that the more significant cause of this artifact was electromotive force. This artifact was called ballistocardiogram. These solutions have enabled interleaving recording wherein EEG recording and fMRI scanning are performed alternatively. Several studies to date on controllable EEG phenomena such as visual evoked potentials (Bonmassar et al., 1999, 2001; Kruggel et al., 2000) and event-related potentials (ERPs) (Kruggel et al., 2001) were conducted using interleaving recording. Many studies have also focused on spike mapping for epilepsy using spike-triggered fMRI (Warach et al., 1996; Krakow et al., 1999; Lazeyras et al., 2000; Lemieux et al., 2001a). However, epileptic spikes, a typical spontaneous EEG phenomenon, cannot be completely captured by interleaving recording.

Second, the imaging artifact in the middle of fMRI acquisition, which has an overwhelmingly spiky waveform, is generated in association with fMRI scanning (Allen et al., 2000; Hoffmann et al., 2000). This artifact markedly interferes with continuous EEG recording during fMRI acquisition. But the necessity of continuous EEG recording to fully observe spontaneous EEG phenomena such as epileptic abnormalities has prompted some laboratories to address this problem, with partial success (Hoffmann et al., 2000; Goldman et al., 2000; Allen et al., 2000), and with actual application to epilepsy (Lemieux et al., 2001b; Salek Haddadi et al., 2002). However, acquisition of EEGs comparable to that recorded in a clinical EEG laboratory is not yet feasible because of the inherent constraints resulting in the frequency dips in multiples of 0.61 and 7.36 Hz (Hoffmann et al., 2000) or limited frequency range up to 40 to 50 Hz (Allen et al., 2000; Hoffmann et al., 2000). In particular, recording EEG phenomena of very low amplitude during fMRI acquisition with sufficient quality for objective evaluation is difficult. This is, for example, reflected by the

estimation that 2 or 3 times of the averaging number was required to observe ERPs (Kruggel et al., 2001).

Given these circumstances, based on the notion that the imaging artifact from the MRI scanner on EEG must have a very different nature from EEG, a typical biological signal, especially in terms of its frequency and amplitude, we observed this artifact with a 20,000-Hz digitization rate and 3000-Hz low-pass filter (LPF) and revealed its detailed characteristics. Based on this observation, we devised a new approach to attenuate the artifact amplitude and retrieve a high-quality EEG signal in the middle of fMRI acquisition. Here we report our initial results from continuous EEG recording with fMRI acquisition, which make available a wider frequency range.

Basic concepts for attenuating imaging artifact

Ballistocardiogram

Ballistocardiogram is an induced current based on Faraday's law, which is caused by ballistic head movement due to cardiac pulsation. We proposed a simple method to suppress the artifact by immobilizing the head with a vacuum cushion system, which was described elsewhere (Anami et al., 2002). We adopted this approach in the present study too.

Imaging artifact

Usually we observe low-pass filtered waveforms of imaging artifacts, e.g., with a DC range up to 100 Hz under a common EEG setup. However, as the artifact is the consequence of sequential RF and gradient pulses working in a microsecond time scale, the original artifact must consist of components with a much higher frequency than those of EEG. To obtain the real waveform of the artifact, we recorded it with 3000-Hz LPF combined with a digitization rate of 20,000 Hz, which eventually enabled observation of the complete waveform of the imaging artifact. An example of an artifact waveform obtained from a typical blip-type fMRI sequence, EPIS sequence (Siemens: ep2d_fid_60b2080_62_64.ekc), is illustrated in Fig. 1. By collating each component of the artifact waveform with the fMRI sequence, it was elucidated that (1) the artifact had complicated but consistent waveforms, and each peak component corresponded precisely to an RF or a gradient pulse, which implies that RF and gradient pulses are major causes of the imaging artifact. (2) The artifacts by gradient pulses (10^3 to 10^4 μV) are much larger than those by RF pulses (up to 10^2 μV) in amplitude, and thus the gradient artifact makes up almost all of the imaging artifact (Fig. 1Ba, b, Ca', b') This result is consistent with that of Hoffmann et al. (2000). The outstanding frequency of the underlying imaging artifact is that of the readout gradient artifact, 833 Hz (period of the readout gradient: 1200 μs); that is, however,
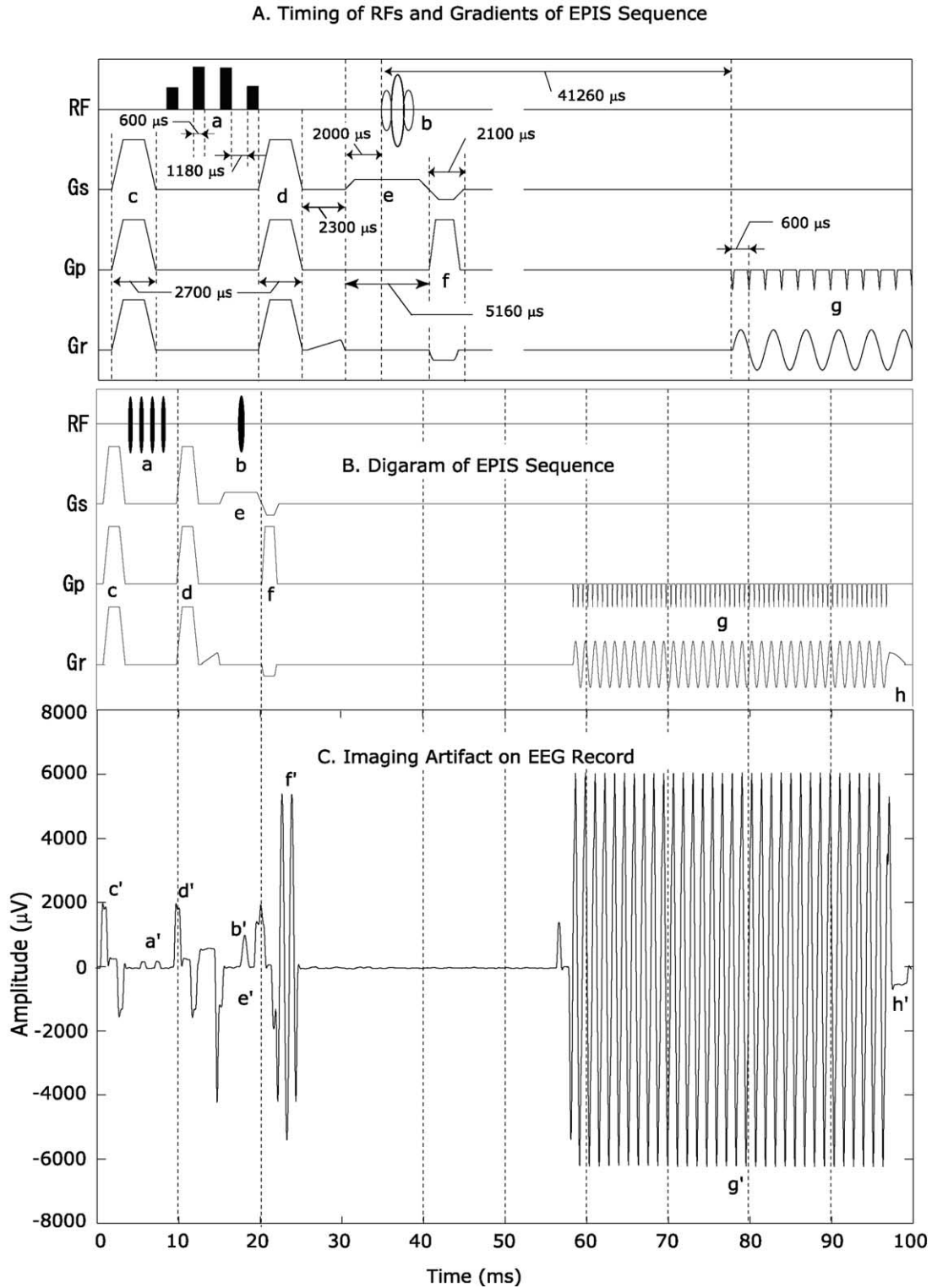
Fig. 1. (A) Timings of RF emission and gradient pulses in an fMRI sequence (EPIS, Siemens: ep2d_fid_60b2080_62_64.ekc) RF, radiofrequency wave; Gs, slice selection gradient; Gp, phase encoding gradient; Gr, readout gradient. a, fat suppression pulses (1-3-3-1 pulses); b, slice selection RF; c, d, h, spoilers; e, slice selection gradient; f, dephasing and rephrasing gradient; g, readout gradient. (B) Schematic diagram of whole EPIS sequence. (C) Imaging artifact waveform for one slice scan on a dummy EEG record with a phantom using the EPIS sequence. The artifact corresponding to each gradient component described above in A can be identified and is denoted by the same alphabet with a prime as that denoting the original gradient.

out of the EEG frequency range and not observable. The observable frequencies within the EEG band were defined by loops of an fMRI sequence that resulted in serious artifacts within the EEG band (Hoffmann et al., 2000). Although an RF emission of 64-MHz resonance frequency is definitely outside a bioamplifier's frequency range, it can cause small artifacts on the EEG record (Fig. 1Ca' and b') (Hoffmann et al., 2000). This seems to be attributable to the fact that the induced current caused by high RF power based on electromagnetic or electrostatic coupling is easily transformed by a demodulation effect in the nonlinear parts in the hardware system into the low-frequency artifact within an EEG amplifier's frequency range and results in artifacts on the EEG record. (3) An artifact component caused by one gradient pulse consisted of a pair of peaks, one of which deflected positively or negatively and the other inversely (Fig. 1Bc, d, 1Cc', d'). This finding supports the contention that gradient artifact is mainly due to electromagnetic coupling (Faraday's law) (Allen et al., 2000; Hoffmann et al., 2000), and thus the artifact from one gradient pulse, in principal, has the differential waveform of the corresponding gradient pulse.

These observations imply that we can predict and control the waveform and time schedule of the artifact. Based on this concept, in order to attenuate the large amplitude of the gradient artifact, we devised a strategy in which when EEG sampling and fMRI scanning are completely synchronized, the differential waveforms of gradient pulses periodically made artifact-free interspaces that allowed EEG sampling with a high signal-to-artifact ratio. Here, this method was called the "stepping stone sampling method" (SSS). After recording the artifacts with SSS, recorded raw data still have residual artifacts, which are subtracted from the averaged artifact to retrieve the EEG signal.

Methods

Subjects and materials

For the phantom study, a bottle-type phantom ($\phi = 12$ cm) filled with cupric sulfate solution was employed. For the human study, five healthy subjects were recruited (two males and three females, average age 32 years old). All five subjects participated in the EEG/fMRI experiment, and one of the female subjects also participated in the fMRI experiment. All subjects provided written informed consent, and the study was approved by the ethics committee of the National Center Hospital for Mental, Nervous, and Muscular Disorders, National Center of Neurology and Psychiatry.

General description of stepping stone sampling

Electrode and cable

Ag–AgCl electrodes attached to metal leads composed of 99.96% copper and 0.04% oxygen were prepared for the

fMRI environment; not only the cables but also the electrode plate were shielded. An electrode plate has another Ag plate that was placed over it with an insulated layer in between and which was connected to the grounding lead (Fig. 2B). The Cz electrode for common reference had as many cables as the number of active electrodes needed to make a twisted pair cable for each of them (Star-burst electrode). Ag–AgCl electrodes were applied to F3, F4, C3, Cz (reference), C4, Pz, O1, O2, A1, and A2 according to the international standard 10–20 system (Fig. 2A). All electrodes were mounted on a custom-made electrode cap. Note that signals from A1 and A2 positioned at bilateral mastoid positions, respectively, referred to the Cz site were recorded as active electrodes. To minimize the distance between the active electrodes and the referential one, all leads first went up to the Cz site, and all of them were twisted with one of the Cz leads and grouped together so that they formed one bundle.

The bunch of cables was carried straight outside the magnet, and the cables went out of the magnet room to be connected to an RF filter. Outside the magnet room, the cables from the RF filter were connected to the head box of the EEG bioamplifier that was electrically floated. EEG was recorded referring to the Cz site.

fMRI sequence programming and acquisition

To achieve the SSS method, the EPIS sequence (the details in Fig. 1A and B) was modified by removing the first spoiler, changing the time schedule (ramp up/down and duration) and amplitude of gradient pulses and RFs. The artifact by RF pulses was found to be much smaller than that by gradient pulses under our fMRI equipment; the former had some hundred microvolts, while the latter had a few thousand microvolts. This finding allowed us to focus on circumventing the artifacts by gradient pulses, ignoring those by RF pulses. Large artifacts are engendered by electromagnetic coupling and assume the same differential waveform as that of the original gradient pulse, with an upward change (ramp up) resulting in a positive peak and a downward change (ramp down) in a negative one. In contrast, when there is a gradient plateau with no such changes, even when the gradient coil is on, in the absence of changes (no ramp up/down), no artifact is produced. However, preliminary experiments revealed that the true, observed results were different from theoretical considerations in the following respects. First, at every transitional point of a gradient pulse from ramp up/down to plateau, or from plateau to ramp down/up, the artifact actually had a slower return to the baseline level than the predicted differential waveform. In fact, it took 600 μs to recover to the baseline level from a peak top. Second, in some cases, in the interval set between a pair of neighboring artifact peaks during which the gradient pulse was on, artifact did not completely return to the baseline level. Instead it preserved a constant value of some hundred microvolts, probably because this kind of

A. Placement of Electrodes
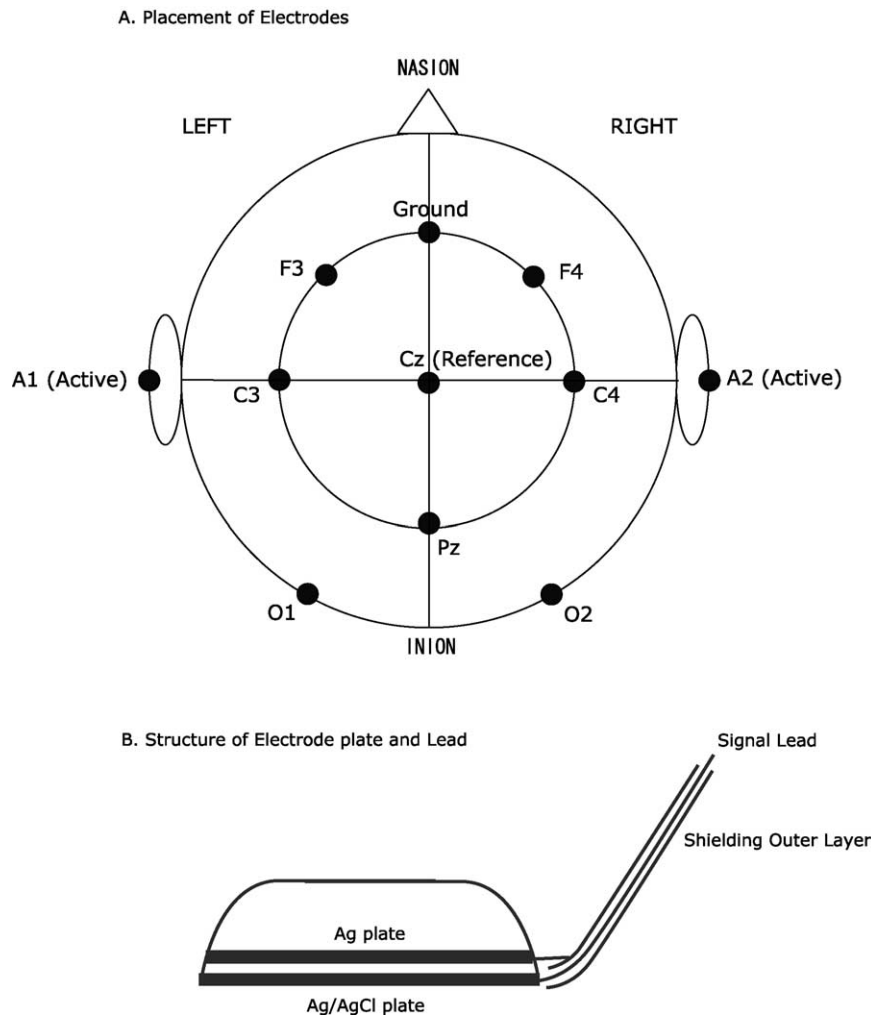

B. Structure of Electrode plate and Lead

Fig. 2. Electrode placement and structure. (A) Electrode placement is based on the standard 10–20 system. (B) Each electrode has double plates inside for shielding.

artifact was caused by electrostatic coupling which under the small stray capacitance had basically a proportional relationship to the gradient pulse waveform. Based on these principles and the actual observations, a new sequence was programmed with a PARGEN (Siemens) compiler so that differential waveforms of the gradient pulses in the sequence had almost artifact-free interspaces at every 1000-μs interval among the artifact peaks, which allowed the EEG to be sampled consistently within those clear interspaces with a 1000-Hz digitization rate (Fig. 3A and B).

Each gradient pulse component was arranged in the above manner. In particular, to realize stable and appropriate EEG sampling in the series of readout gradient artifacts, 400 μs still time was added at every peak top of the sine wave gradient pulses. This provided a near-baseline interspace by differential procedure (Faraday's law), a "sampling shelf" that was long enough for EEG to be digitally sampled in a resultant readout gradient artifact (Fig 3D). This sequence was called the stepping stone sequence. Fig.

3A and B showed that EEG sampling points at a 1000-Hz digitization rate drop in baseline interspaces on the differential gradient waveform of the stepping stone sequence all the time. The details of the timing and the parameters of the sequence are listed in Fig. 3A, C, and D. The bandwidth of the readout gradient was 1136 Hz. The position of an electrode and a related circuit defines polarity (positive or negative) and the amplitude of individual imaging artifacts on the EEG record, leading to a variety of artifact waveforms across the multiple channels. However, the fact that the time schedule of gradient ramp up/down is the same across the channels in combination with the Sample/Hold mechanism of the EEG amplifier assures phase-locked EEG sampling across the channels, with the stepping stone sampling working across the multiple channels. As described above, the actually recorded artifact is, however, somewhat different from the theoretical prediction. Slow recovery to the baseline level can be treated by putting additional time shift in a sequence, but the problem of persisting potential
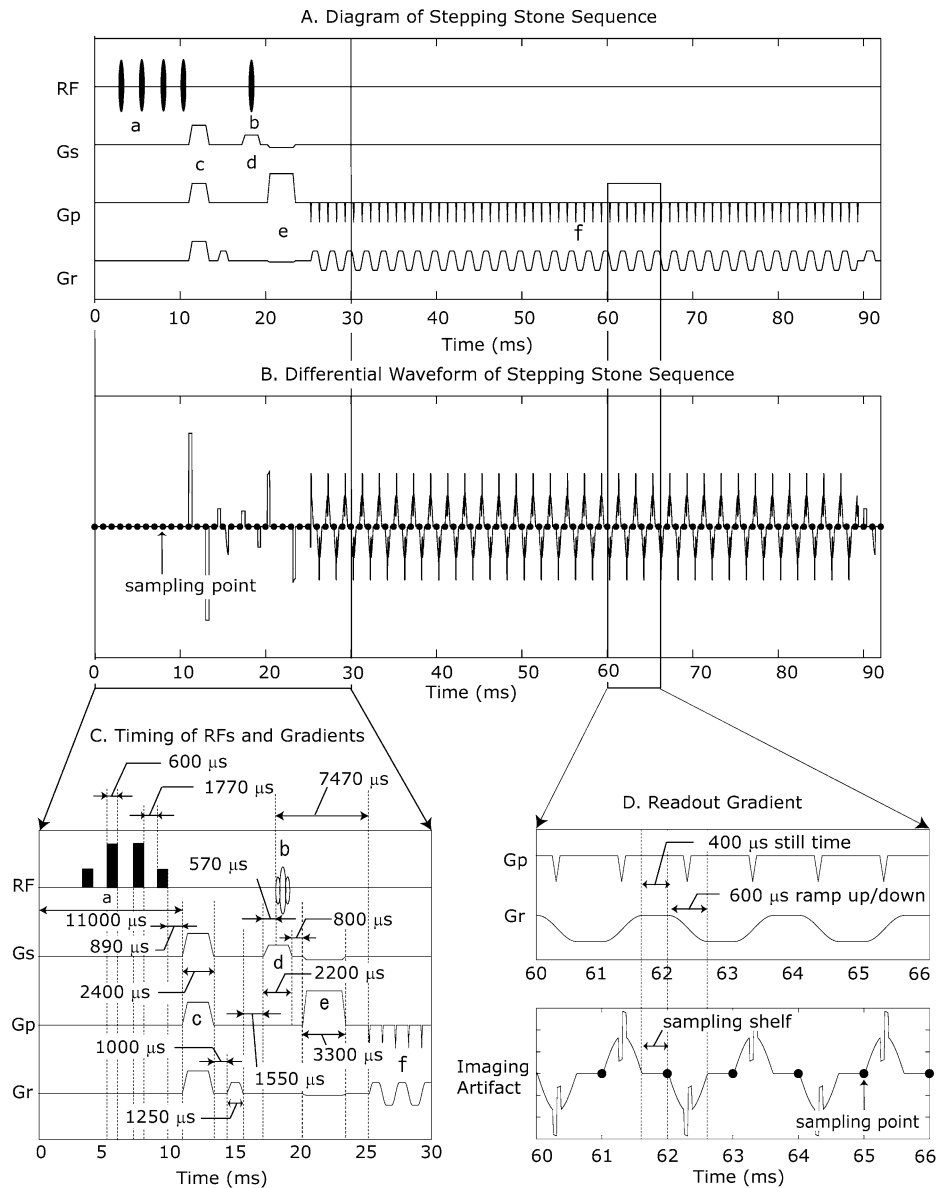
Fig. 3. Schematic diagram of the stepping stone sequence. (A) Diagram of the series of RF and gradient pulses in the stepping stone sequence is illustrated. RF, RF pulses; Gs, slice selection gradient; Gp, phase encoding gradient; Gr, readout gradient; a, fat suppression pulses; b, slice selection RF; c, spoiler; d, slice selection gradient; e, dephasing and rephasing gradient; f, readout gradient. (B) An example of predicted imaging artifact waveform made by sum of the differential waveforms of the each gradient pulses (Gs, Gp, Gr). Digitally sampled dots for EEG signal (1000-Hz digitization rate) are superimposed on the artifact waveform. Every sampling point avoids artifact spikes. (C) Magnified figure of the former part of A. Timings of RFs and gradient pulses are illustrated. (D) Magnified figure of the readout gradient of A. A 400-μs still time on the top of the readout gradient results in the sampling shelf in the imaging artifact that allows stable phase-locked EEG sampling.

hanging over the baseline is difficult to solve perfectly, which results in high-frequency artifacts. Most of these can be filtered out by LPF, but low-amplitude artifacts persist on the data. This requires an additional post hoc artifact correction procedure.

fMRI acquisition was conducted on a 1.5-T MRI scanner with a circular polarization coil (Siemens Magnetom Vision Plus, Siemens, Erlangen, Germany). Acquisition was manually started, which also immediately initiated EEG sampling via a trigger sent from the MRI scanner.

EEG acquisition

For EEG recording, a digital amplifier, 32ch. SynAmps (Neuroscan Lab, Sterling, VA, USA) controlled by the SCAN4.2.1 program installed in a PC (Pentium III 600 MHz) was employed. EEG data were sampled at a 1000-Hz digitization rate and with 0.336 μV/bit amplitude resolution and a dynamic range of 22 mV. According to our experiments, 1-μs shift of EEG sampling sometimes made a 70-μV difference in the underlying imaging artifact during the readout gradient. This fact implied that for phase-locked

sampling EEG data within near-baseline interspaces, almost microsecond order precision and temporal consistency in synchronization of EEG data sampling together with gradient pulse firing would be required. Accordingly, we adopted a single clock driving the whole EEG/MRI system by driving SynAmps with the MRI scanner's clock, which assured good phase-locked EEG sampling. For performing external Sample/Hold in SynAmps, Neuroscan's standard procedure was completed (see http://www.neuro.com/ext_sh.htm). For modifying too high a frequency of the MRI scanner's internal clock (4 MHz) to the acceptable frequencies for SynAmps driving, a clock divider, CD-2 (Physio-Tech, Tokyo, Japan), was used which down sampled the original frequency to provide several clock frequency options (1000, 2000, 10,000, 20,000 Hz) to drive the SynAmps. The data were sampled at a 1000-Hz digitization rate with 10,000 Hz of the external clock provided by CD-2 and had 2000 Hz of the cutoff frequency of the anti-aliasing filter.

The very high cutoff frequency makes the imaging artifacts sharp and high with a narrow width, which on the other hand provides wide near-baseline interspaces among artifact spikes that make sampling at the near-baseline interspaces much easier. However, this recording condition can cause aliasing contaminations on the EEG record, although in practice aliasing does not cause a major problem, as is further discussed in the Appendix.

The first EEG sampling point on the fMRI sequence at the start of simultaneous recording fixes the phase-locked point and determines how high the amplitude of the imaging artifact remains in the rest of the underlying recording. This implies that accurate alignment of the starting point of the fMRI scanning and EEG sampling is necessary. For this purpose, a trigger from the MRI scanner embedded at the head of the fMRI sequence was sent to CD-2 to initiate data sampling. If necessary, an additional detailed adjustment could be performed in CD-2 that allowed modification of the sampling starting point with a 0.125-μs interval.

EEG postprocessing

All EEG signal processing was implemented on Matlab (Mathworks, Inc., MA, USA). Residual artifact was subtracted from the averaged artifact template. Every subtraction point is determined precisely by TR, because the EEG amplifier was driven by the MRI scanner's clock. A 100-ms span of data prior to the first point, whole data of one volume scan, and the following data of the next 300 ms were grouped together and averaged across all volumes to make an averaged artifact template. Fifty milliseconds of data prior to the starting point was used to determine the baseline level. The template was eventually subtracted from every artifact on data for each channel basis. Following the subtraction, the data of all channels were filtered out by elliptic LPF. If necessary, the reference can be changed. For mastoid reference, from raw data, (AR − Cz), (AL − Cz), (A1 − Cz), (A2 − Cz), (AL − CZ) − (A1 − Cz) = AL − A1, (AR − Cz) − (A2 − Cz) = AR − A2, where AR denotes an active electrode on the right scalp and AL one on the left scalp. Similarly for linked mastoid reference, (AR − Cz) − (1/2) × {(A1 − Cz) + (A2 − Cz)} = AR − (1/2) × (A1 + A2).

Notes on individual experiments

The experiments in this study are subdivided into three parts: a stepping stone sequence validation experiment, an experiment with a phantom, and one with a human for EEG/fMRI.

Validation of the stepping stone sequence

To verify whether the stepping stone sequence is sufficiently sensitive for BOLD contrast, we compared fMRI activation by the stepping stone sequence with that by EPIS sequence (Siemens: ep2d_fid_60b2080_62_64.ekc) using a visual stimulation paradigm without simultaneous EEG monitoring. EPIS sequence is a FID-type (gradient echo type) sequence (64 matrix, readout bandwidth 2080 Hz), featuring fast image acquisition with mosaic image format. This sequence is composed of spoiler–fat suppression pulses (1-3-3-1 pulses)–spoiler–slice selection pulse–dephasing and rephasing pulses–readout pulse–spoiler, in this order (Fig. 1A and B). One subject was recruited for this experiment. Two sessions were performed on different days with a 1-week interval for the test–retest experiment. Checkerboard visual stimulation (8 Hz, 8 × 8 matrix) was employed for task blocks and hairline cross fixation for control blocks. Stimuli were displayed on the screen from an LCD projector, introduced into the MRI gantry, and presented to the subject via a mirror mounted on the head coil. One block had 10 volume scans, and one run consisted of 10 blocks that were preceded by 10 dummy scans. Task and control had 5 blocks, respectively. Functional images were collected in two runs: one with EPIS sequence (TR = 3000 ms, TE = 60 ms, flip angle = 90°, FOV: 192 mm, 64 × 64 image matrix) and the other with the stepping stone sequence (TR = 3000 ms, TE = 60 ms, flip angle = 90°, FOV: 192 mm, 64 × 64 image matrix). From each of the runs, 100 sets of 20 slices, 6-mm-thick axial images, with 0.6 mm gap in between parallel to the anterior–posterior commissure plane covering the whole brain were acquired. Data analysis was performed with SPM99 (Wellcome Department of Cognitive Neurology, London, UK). fMRI data were treated with realignment and smoothing with Gaussian kernel with 8-Hz FWHM, after which statistical analysis was performed using a general linear model, with statistical significance defined as corrected $P < 0.05$. The global maximum point was obtained on the statistical result. Separately, the smoothed Analyse format image files (not realigned) were read in on Matlab for the following procedures. Then, in the vicinity of the global maximum point, the ROI with a dimension of 9 mm (3 voxels on x axis) × 9 mm (3 voxels on y axis) × 6 mm (1 voxel on z axis)
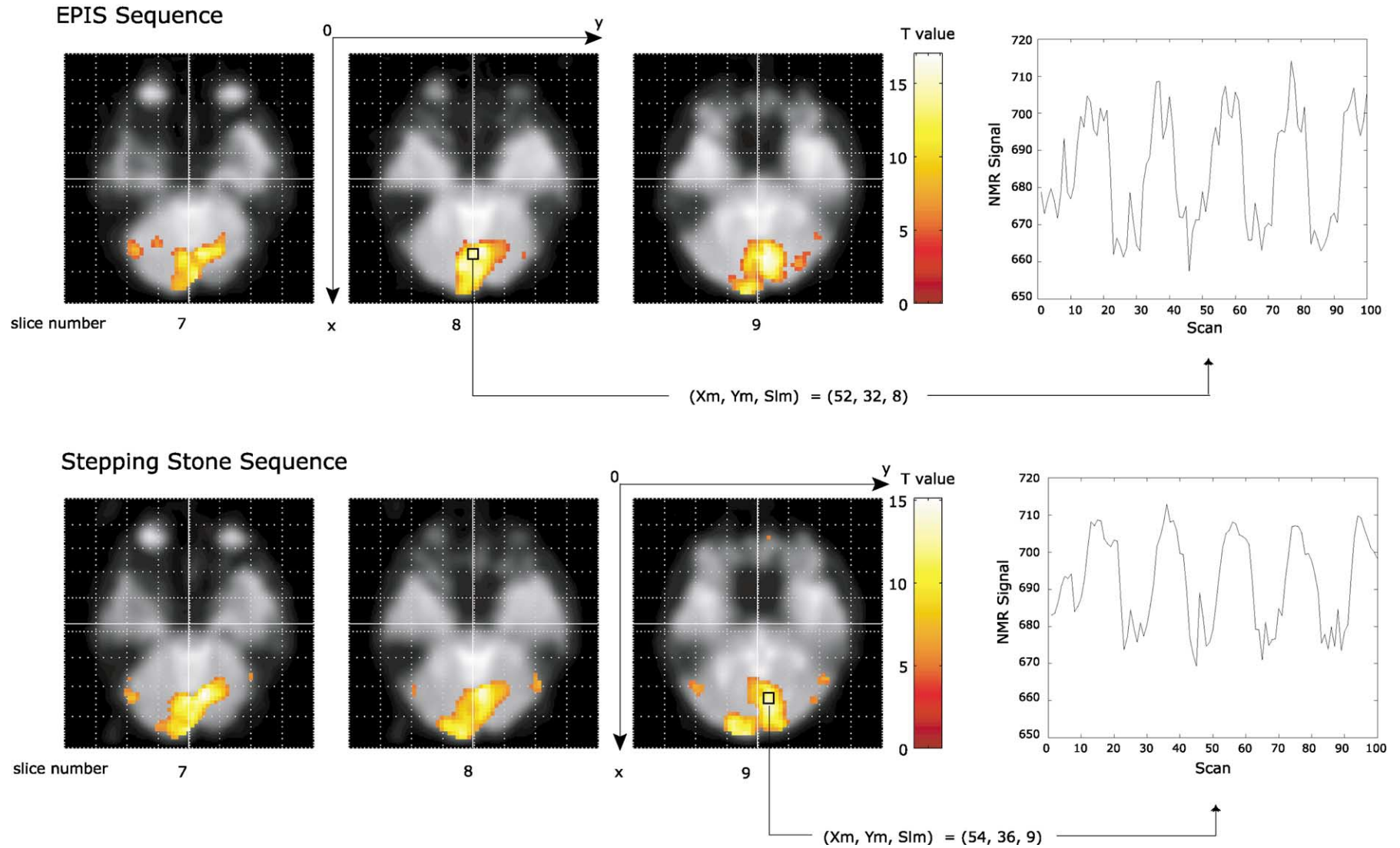
Fig. 4. Activated areas in occipital lobe from the first experiment were demonstrated with the EPIS and the stepping stone sequence. The time courses of the NMR signal with the two sequences were also demonstrated. Xm, Ym, and Slm denote the coordinate and the slice number of the ROI that showed the maximum percentage change in the NMR signal between the task/control blocks.
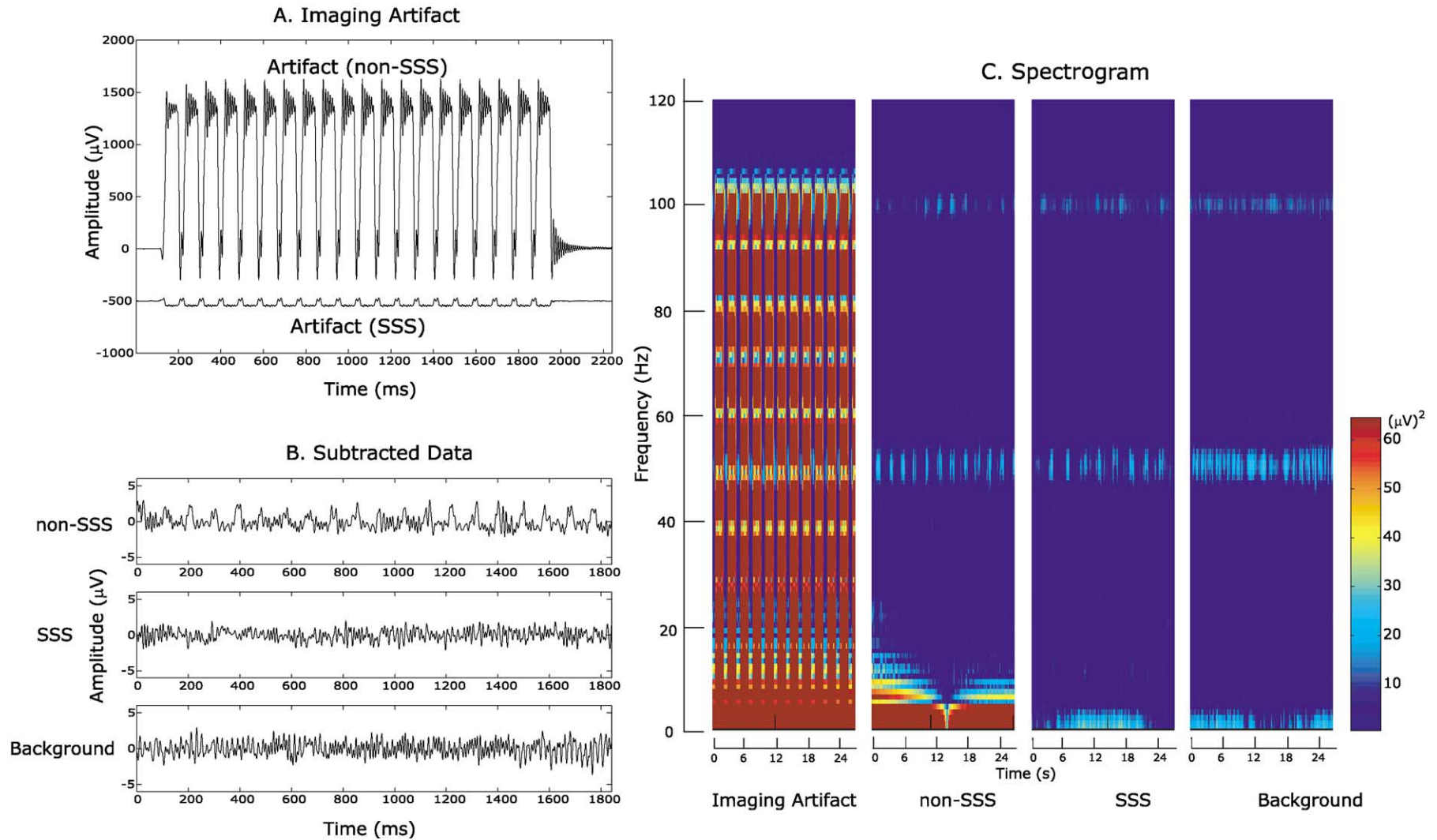
Fig. 5. Imaging artifact and residues after artifact subtraction in SSS and non-SSS acquisition. A. Imaging artifact: averaged artifact on a phantom from SSS and non-SSS acquisition in which 20 slices for one volume scan were obtained. Large series of artifact peaks are of non-SSS acquisition, whereas the smaller one is of SSS acquisition. B. Subtracted data: the data during one volume scan (20 slices, 1840 ms) after averaged -artifact subtraction were illustrated in non-SSS and SSS acquisition. Background noise for the same span is also displayed for reference. C. Spectrogram: specgram.m program in Matlab modified to display power was used for temporal FFT analysis. Temporal FFT profiles (from DC up to 100 Hz) of subtracted data are illustrated for non-SSS and SSS, as well as imaging artifact and background noise. The color map demonstrates a power spectrum for 27 s of fMRI scans. In this color code the hotter the color the higher the power. Weak spectral power bands observable at 50 and 100 Hz are hum noise and its harmonics, respectively.

Table 1
First: result from the first experiment of fMRI acquisition; second: result from the second experiment conducted a week after the first with the same subject

	EPIS sequence		Stepping stone sequence	
	First (Xm, Ym, Slm)	Second	First (Xm, Ym, Slm)	Second
Percentage signal change (%)	4.27 (52, 38, 8)	3.75 (50, 42, 7)	3.42 (54, 36, 9)	3.55 (54, 39, 7)
S/N ratio	42.2	38.0	50.4	44.4

Note. Xm, Ym, and Slm denote the coordinate and the slice number of the ROI that showed the maximum percentage change in the NMR signal between the task/control blocks.

showing the maximum percentage change in the NMR signal between the task and the control blocks was detected in each run. The S/N ratio was obtained from the signal of an ROI in white matter (signal value) and that in an empty space near the upper right edge (noise value) of the image matrix.

EEG/fMRI experiment with a phantom

In order to estimate to what extent the amplitude of imaging artifact is reduced by the SSS method and how the smaller artifact acquired with it facilitates retrieval of the EEG signal from among various imaging artifacts, imaging artifacts on one channel of the EEG record were compared between the SSS and non-SSS methods with the stepping stone sequence and one clock driving but without start alignment wherein stepping stone sampling did not work, but artifacts with similar characteristics could be obtained. The phantom surface was coated with EEG paste to create an electrical circuit composed of active, referential, and ground electrodes. The circuit extended halfway around the bottle, whose aperture area was approximately 55 cm^2 set vertically to the z axis direction in the magnetic field. Impedance was adjusted to less than 1 kΩ. Forty volume scans were recorded in both of these sessions. Data were filtered with 100-Hz LPF, and each artifact was subtracted from the averaged artifact that was averaged across the last 25 volume artifacts.

EEG/fMRI experiment with a human subject

Continuous EEG/fMRI was recorded with five human subjects. One hundred volumes each consisting of 20 axial slices (5 mm thickness, no gap; TE: 40 ms; TR: 3000 ms; FOV: 192 mm; 64 × 64 image matrix) were acquired using the SSS method. To suppress the ballistocardiogram, the vacuum head fixation system (Med-Tec Co., USA) was employed. In the inflated (soft) condition, it can mold to the subject's head shape. Once it is deflated, it becomes solid but continues to retain the subject's head's shape precisely and thus can immobilize the head in a comfortable position. Unlike the soft and elastic cushions or puddings usually used in fMRI experiments for head fixation, the solidity and close contact with the whole head achieved with this system effectively suppress the head's microvibrations leading to substantial attenuation of the ballistocardiogram to an acceptable level. Actually the plastic bag pillow filled with small plastic particles was set to fill in the clearance gap between the subject's head and the head coil. Next, the air in the pillow was deflated so that the subject's head was properly fixed and comfortably supported in the head coil. Deflation was adjusted to suppress the head's microvibration by observing the ballistocardiogram on the EEG. Impedance at all electrodes was preserved at less than 10 kΩ.

Results

Validation of the stepping stone sequence

The SPM {T} showed the activations in the bilateral occipital areas in both results with the stepping stone sequence and the EPIS sequence with the checkerboard stim-

Table 2
Remnants of imaging artifact with the SSS method and α activity outside/during fMRI acquisition

	Amplitude of imaging artifact	α wave ouside magnet		α wave during fMRI acquisition	
	Average ± Standard deviation (Median) (μV)	Average amplitude (μV)	Standard deviation (μV)	Average amplitude (μV)	Standard deviation (μV)
Subject					
1	160.9 ± 135.7 (141.0)	64.6	8.9	72.2	10.1
1	160.9 ± 135.7 (141.0)	64.6	8.9	72.2	10.1
2	102.2 ± 40.0 (104.5)	96.0	18.3	95.8	31.5
3	153.2 ± 80.5 (156.8)	94.3	11.4	106.0	22.3
4	163.2 ± 73.5 (187.3)	62.2	10.8	61.1	10.7
5	143.1 ± 85.6 (156.5)	58.1	14.2	60.0	10.2

Note. Statistics of peak-to-peak amplitude of residual imaging artifact across the channels and statistics of peak-to-peak amplitude of consecutive 20 α waves at the O2 position outside magnet/during fMRI acquisition are shown.
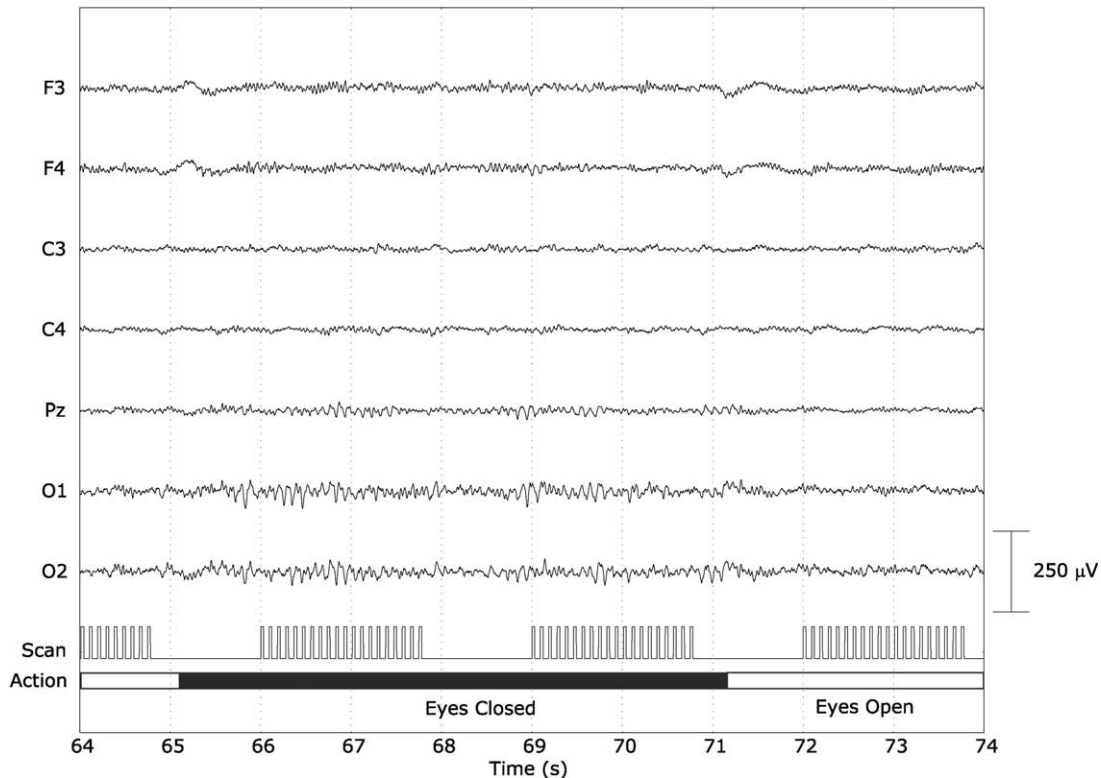
Fig. 6. Retrieved time domain EEG record from 0.8 Hz up to 100 Hz during fMRI acquisition. Seven channels of retrieved EEG data referred to Cz for 10 s after artifact correction are illustrated. During the middle two scans, a subject closed his or her eyes, while he or she opened them within scans at both ends. α activity was augmented during eyes-closed periods, while β activity was predominant during eyes-opened periods.

ulation paradigm (Fig. 4). The time course of the ROI showing the maximal percentage signal change between the task/control blocks with the two sequences is also demonstrated in Fig. 4.

The result of the maximal percentage change in the NMR signal between the task/control blocks and S/N ratio is shown in Table.1. The percentage change was better with the EPIS sequence, while the S/N ratio was better with the stepping stone sequence.

EEG/fMRI experiment with the phantom

Fig. 5A demonstrates the artifact waveform from SSS and non-SSS acquisition. Averaged peak-to-peak amplitude of the imaging artifact from one volume SSS acquisition was 83.9 ± 1.4 μV, while non-SSS was 1910.5 ± 28.0 μV. Fig. 5B illustrates the data from non-SSS, SSS, and background noise, respectively, after artifact correction. The data from non-SSS still had remaining artifacts whose frequency was slightly more than 10 Hz. In fact, the stepping stone sequence with 40 ms of TE requires 92 ms for one slice scan, leading to 10.87-Hz periodicity for a multislice scan in consequence, which was reflected by the frequency of the residual artifact on non-SSS data. In contrast, SSS appeared to have no observable residue arising from the imaging artifact, but the amplitude of the noise in SSS looked smaller than the background noise. The spectrograms in Fig. 5C reveal that the background data had a

greater amount of 50-Hz hum noise than that of SSS. Accordingly, the underlying amplitude difference is probably caused by the phenomenon that 50-Hz hum noise often happened to be phase-locked with the MR scanner's internal clock, with subtraction correction often attenuating hum noise as well, leading to less residual noise in SSS than background noise. The spectrograms also show that imaging artifact existed over almost all frequency ranges. In non-SSS acquisition, although the result of subtraction in the high-frequency band appeared to be successful in this case, there were still some residual artifact powers observable at lower frequencies less than 12 Hz. In contrast, subtracted data from SSS acquisition were very similar to those from background noise, assuring that almost all imaging artifacts were successfully removed.

EEG/fMRI experiment with human subjects

The EEG data were acquired from continuous EEG/fMRI recording with SSS method. The acquired data were treated with LPF (100 Hz). Table 2 showed the averaged amplitude of remnants of imaging artifact across the seven channels (F3 − Cz, F4 − Cz, C3 − Cz, C4 − Cz, Pz − Cz, O1 − Cz, O2 − Cz) and the retrieved α activity on O2 during fMRI acquisition after artifact correction for each subject. α activities recorded outside the magnet were also demonstrated for comparison with that during fMRI acquisition. All averaged artifact amplitudes were less than 165
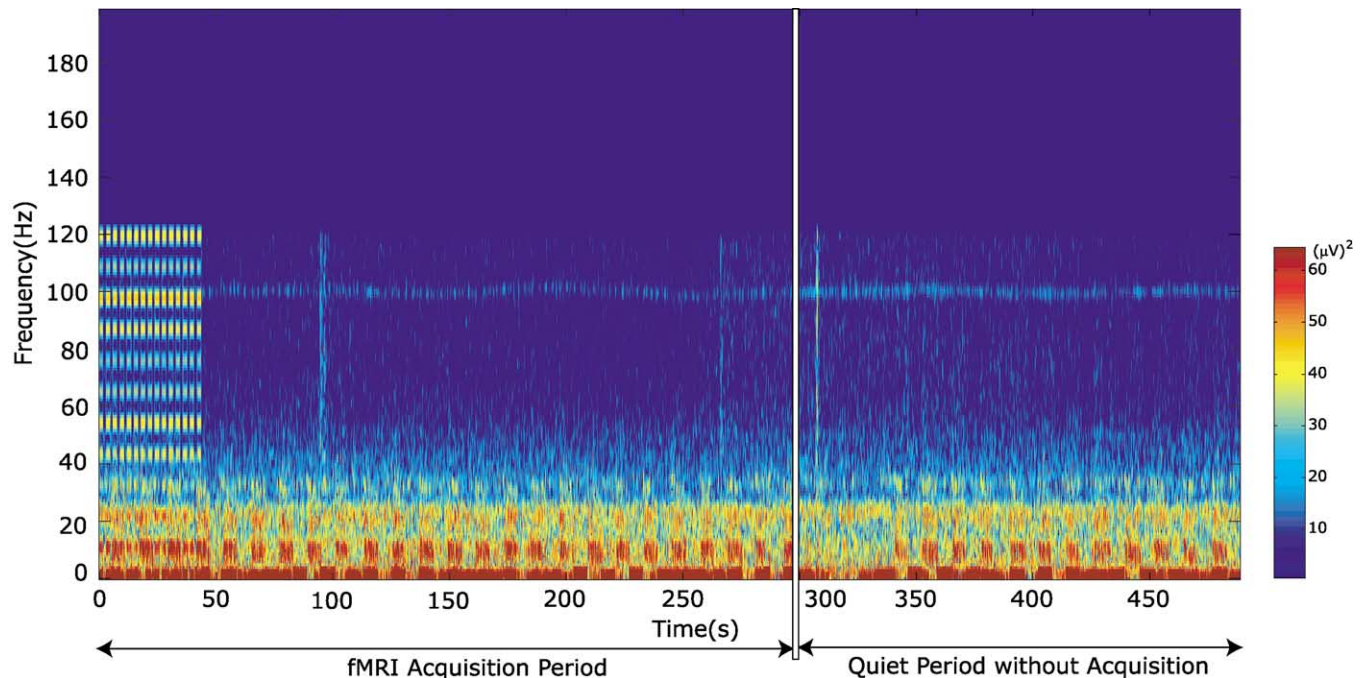
Fig. 7. Spectrogram of human EEG during 100 volumes acquisition. Temporal FFT result of the whole EEG data on O2 site of the same experiment as shown in Fig. 6 is illustrated. The modified specgram.m in Matlab was used. Subject was instructed to open/close his or her eyes every 2 volume scans alternatively. The first 15 scans had no artifact correction so as to demonstrate the original artifacts. The next 85 scans were artifact corrected. After fMRI acquisition, EEG continued to be further recorded for the next 3 min. The subject once stopped open/close eyes behavior at the end of fMRI acquisition and resumed it 1 min later. Harmonic hum noise was weakly visible around 100 Hz.

μV which was approximately 1/10 of a common artifact amplitude in EEG recording during fMRI acquisition.

Fig. 6 showed the actual time domain EEG data for 10 s after artifact correction. Attenuation/augmentation of α activity was observable during the eyes open/closed period, respectively.

Temporal FFT analysis on EEG signal was performed on Matlab throughout 100 volume scans (5 min). A subject was instructed beforehand to open/close his or her eyes spontaneously at every 2-volume scan interval. Fig. 7 demonstrates the result on the O2 site. For reference, the first 15 scans did not have any artifact correction. During this period, imaging artifacts were displayed as periodical sharp bands over most frequency ranges. During the last 85 scans (from the end of the imaging artifact until 300 s), the augmentation/attenuation of alpha activity during the eyes opened/closed periods was clearly demonstrated with the striped pattern around 10 Hz in which the hotter color designated the more augmentative alpha activity. The FFT profile from DC up to 120 Hz during the last 85 scans was very similar to the profile without scanning (from 300 s until the end of the record).

Discussion

Imaging artifacts from the echo-planar sequence differ markedly from biological signals in terms of their frequency and amplitude. The very high digitization rate and high cutoff frequency in LPF revealed its real waveform and elucidated that the artifact precisely traced the components of the echo-planar sequence. Due to the fiercely deflecting waveform, even a small shift in data sampling can change the consequent artifact waveform. Artifacts cannot be precisely subtracted with averaged artifacts, unless each scan has a very similar waveform. We solved this problem with the one-clock driving that controlled the whole EEG/fMRI system and with the start alignment of EEG sampling and fMRI sequence using trigger starting.

The artifact observation also revealed that the real amplitude of the artifact could be 40 mV in our MRI equipment, which seems to be in concordance with a theoretical calculation at 2 Tesla (Allen et al., 2000). This high voltage leads to potential data overflow out of the amplifier dynamic range. However, such a low cutoff frequency in LPF as widely used in clinical EEG examinations strongly attenuates and smoothes the high-frequency artifact and thus, critically, LPF may conceal the artifact clipping and result in apparently misleading data. Allen et al., (2000) solved the overflow problem by putting a 70-Hz LPF following a small gain differential amplification, which can substantially attenuate the artifact's amplitude to keep it within the amplifier's dynamic range. The SSS method can be an alternative solution, which is, in principle, irrespective of the amplifier's dynamic range, because the sampling is performed exclusively within the periods in which the signal resides

around the baseline. In other words, regardless of the height of the original artifact amplitude, data can be obtained consistently within the amplifier's dynamic range. According to the result of the phantom experiment described above, the small artifact amplitude contributes to less residual imaging artifact on EEG data after artifact correction. Furthermore, the irrelevancy to artifact amplitude permits a large amplifier gain that has a higher amplitude resolution, which is important especially to estimate low-amplitude EEG phenomena such as ERPs.

The SSS method had a substantial effect on attenuating the imaging artifact amplitude. Actually it attenuated the artifact amplitude to less than 1/22 of the original one in the present phantom experiment. This effect actually contributed to the precision in the averaged artifact subtraction procedure, which is important because multiple slice scans in which a single slice scan requires 80 to 100 ms for acquisition commonly result in large peak artifacts of 10 to 12 Hz in frequency, so that the residues due to such incomplete artifact subtraction also have a similar frequency, thereby sometimes mimicking α activity on human EEG records.

According to our experiments, 1-μs shift of EEG sampling sometimes makes a 70-μV difference in the underlying imaging artifact during the readout gradient. Hence the sampling shelf assures stable EEG sampling exclusively during near-baseline among the fiercely fluctuating artifact spikes caused by the readout gradient. On the other hand, the sampling shelf broadens the readout gradient span (64 ms), which can give rise to disadvantages with the SSS method: (1) a possibility of distorting BOLD contrast images especially in basal forebrain, (2) a longer acquisition time for an fMRI run, (3) slightly lower percentage signal change between the task/control blocks. To compensate for these disadvantages, rather short TE should be used for the SSS method. On the other hand, the narrow bandwidth contributes to good S/N ratio on fMRI images and low amplitude of imaging artifact on the EEG record contributes to good-quality EEG.

To sample EEG data within the sampling shelves together with the 1000-Hz digitization rate, the combination of 300-μs ramp up–400-μs still time–300-μs ramp down in readout gradient pulses is required using the Siemens Vision Plus scanner. However, this combination constraint can be improved by high-speed gradient capability and more digitization rate options in an EEG amplifier. That is, the faster gradient speed in combination with an appropriate digitization rate facilitates the shorter readout gradient span leading to a shorter fMRI acquisition time and no concern about potential image distortion. For example, 200 μs–225 μs–200 μs in combination with a 1600-Hz digitization rate results in a 40-μs readout gradient span.

In conclusion, the present technological innovation has enabled us to obtain good-quality EEG data even under the unfavorable condition of fMRI acquisition. Accordingly, broad practical utilization of both high-quality EEG and concomitant brain hemodynamic mapping through fMRI can provide a new understanding of the generating systems of various spontaneous EEG activities such as basic waves (α, β, and γ waves), epileptic spikes, and sleep hump and spindle waves, as well as those of ERP components, in terms of anatomical substrates apart from the volume conduction mechanism of electricity.

Appendix

In the SSS method, data sampling with a 1000-Hz digitization rate (Fs) with 2000 Hz of high cutoff frequency in the anti-aliasing filter (the highest frequency included in the data (Fh) = 3000 Hz) was used. Then,

$$\text{Nyquist frequency} = (1/2) \times \text{Fs} < \text{Fh}.$$

Accordingly, this condition violates the sampling theorem, and thus the acquired data should have aliasing contamination. The aliasing contamination is defined by the data components of which frequencies are higher than the Nyquist frequency. For estimating the aliasing contamination, human EEG data in a magnet with (B)/without (A) fMRI acquisition at a 20,000-Hz digitization rate with 3500-Hz high cutoff frequency of LPF in the SynAmps preamplifier were recorded. The data during fMRI acquisition were artifact corrected with averaged artifact subtraction. In Fig. 8A and B, the power spectrum density of the data is demonstrated. Both EEG data had 105 $(\mu\text{V})^2$ of EEG signal peaks at around 10 Hz and had less than 0.6 $(\mu\text{V})^2$ of components up to 10,000 Hz (Nyquist frequency of the digitization rate) except the one at 600 Hz (see the magnified figures inside. The range from 1000 to 10,000 Hz not shown in the figure). The underlying 600-Hz component was clearly visible and could cause substantial aliasing contamination in the data recorded at 1000 Hz digitization rate with the SSS method. However, the aliasing by the components at Fa Hz ranging from the Nyquist (500 Hz) to 900 Hz including the outstanding 600-Hz component can emerge at the frequency (1000-Fa) Hz ranging from 100 to 500 Hz that are higher than our interest of EEG data frequency range and, thus, can be eliminated by a usual LPF procedure. Next, the actual alias contamination was estimated by EEG inspection using the above data in a magnet. Two sets of data were derived from the data using the different procedures. Alias-clean EEG was first low-pass filtered with 80 Hz and subsequently down sampled at a 1000-Hz digitization rate. Alias-contaminated EEG was first down sampled to 1000 Hz and subsequently low-pass
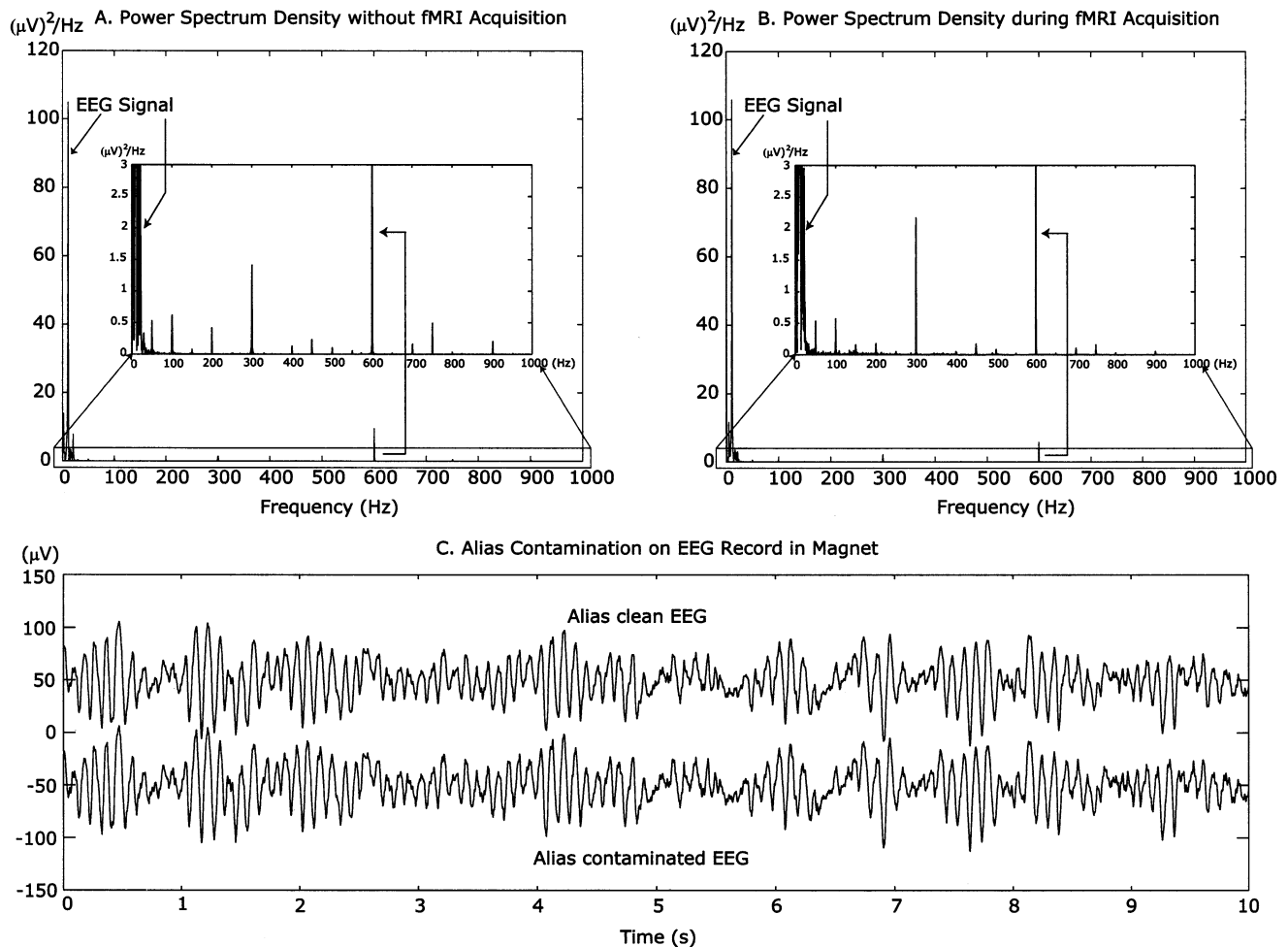
Fig. 8. (A) Power spectrum density on human EEG data recorded inside magnet without fMRI acquisition. The longitudinal axis is magnified in the small figure inside for easy detailed observation. (B) Power spectrum density on the same human EEG as (A) inside magnet with fMRI acquisition. The imaging artifacts were corrected with averaged artifact subtraction. (C) The waveforms obtained through two different estimation methods on the human EEG data. The upper waveform is the alias-clean EEG, while the lower one is the alias-contaminated EEG.

filtered with 80 Hz, which should have alias contamination. Fig. 8C demonstrates these alias-clean/contaminated EEG data in parallel. It was found that there was no apparent difference between them with inspection. From this result, it was concluded that aliasing contamination did not substantially interfere with EEG observation during fMRI acquisition using the SSS method.

References

Allen, P.J., Polizzi, G., Krakow, K., Fish, D.R., Lemieux, L., 1998. Identification of EEG events in the MR scanner: the problem of pulse artifact and a method for its subtraction. NeuroImage 8 (3), 229–239.

Allen, P.J., Josephs, O., Turner, R., 2000. A method for removing imaging artifact from continuous EEG recorded during functional MRI. NeuroImage 12 (2), 230–239.

Anami, K., Saitoh, O., Yumoto, M., 2002. Reduction of ballistocardiogram with a vacuum head-fixating system during simultaneous fMRI and multi-channel monopolar EEG recording. Int. Congr. Se. 1232, Recent Adv. Hum. Brain Mapp. 1232, 427–431.

Belliveau, J.W., Kennedy Jr., D.N, McKinstry, R.C., Buchbinder, B.R., Weisskoff, R.M., Cohen, M.S., Vevea, J.M., Brady, T.J., Rosen, B.R., 1991. Functional mapping of the human visual cortex by magnetic resonance imaging. Science 254, 716–719.

Bonmassar, G., Anami, K., Ives, J., Belliveau, J.W., 1999. Visual evoked potential (VEP) measured by simultaneous 64-channel EEG and 3T fMRI. Neuroreport 10 (9), 1893–1897.

Bonmassar, G., Schwartz, D.P., Liu, A.K., Kwong, K.K., Dale, A.M., Belliveau, J.W., 2001. Spatiotemporal brain imaging of visual-evoked activity using interleaved EEG and fMRI recordings. Neuroimage 13 (6), 1035–1043 Pt. 1.

Goldman, R.I., Stern, J.M., Engel Jr., J., Cohen, M.S., 2000. Acquiring simultaneous EEG and functional MRI. Clin. Neurophysiol. 111 (11), 1974–1980.

Hoffmann, A., Jager, L., Werhahn, K.J., Jaschke, M., Noachtar, S., Reiser, M., 2000. Electroencephalography during functional echo-planar imaging: detection of epileptic spikes using post-processing methods. Magn. Reson. Med. 44, 791–798.

Krakow, K., Woermann, F.G., Symms, M.R., Allen, P.J., Lemieux, L., Barker, G.J., Duncan, J.S., Fish, D.R., 1999. EEG-triggered functional MRI of interictal epileptiform activity in patients with partial seizures. Brain 122, 1679–1688 (Pt. 9).

Kruggel, F., Wiggins, C.J., Herrmann, C.S., von Cramon, D.Y., 2000. Recording of the event-related potentials during functional MRI at 3.0 Tesla field strength. Magn. Reson. Med. 44 (2), 277–282.

Kruggel, F., Herrmann, C.S., Wiggins, C.J., von Cramon, D.Y., 2001. Hemodynamic and electroencephalographic responses to illusory figures: recording of the evoked potentials during functional MRI. NeuroImage 14 (6), 1327–1336.

Lazeyras, F., Blanke, O., Perrig, S., Zimine, I., Golay, X., Delavelle, J., Michel, C.M., de Tribolet, N., Villemure, J.G., Seeck, M., 2000. EEG-triggered functional MRI in patients with pharmacoresistant epilepsy. J. Magn. Reson. Imaging 12 (1), 177–185.

Lemieux, L., Krakow, K., Fish, D.R., 2001a. Comparison of spike-triggered functional MRI BOLD activation and EEG dipole model localization. NeuroImage 14 (5), 1097–1104.

Lemieux, L., Salek Haddadi, A., Josephs, O., Allen, P., Toms, N., Scott, C., Krakow, K., Turner, R., Fish, D.R., 2001b. Event-related fMRI with simultaneous and continuous EEG: description of the method and initial case report. NeuroImage 14 (3), 780–787.

Salek Haddadi, A., Merschhemke, M., Lemieux, L., Fish, D.R., 2002. Simultaneous EEG-correlated Ictal fMRI. NeuroImage 16, 32–40.

Warach, S., Ives, J.R., Schlaug, G., Patel, M.R., Darby, D.G., Thangaraj, V., Edelman, R.R., Schomer, D.L., 1996. EEG-triggered echo-planar functional MRI in epilepsy. Neurology 47 (1), 89–93.